HEAT BALANCE AND THERMAL CONDUCTION

G. KOCKARTS
Institut d'Aéronomie Spatiale de Belgique, 3 Avenue Circulaire, B-1180 Bruxelles, Belgium

1. Introduction

A large amount of information regarding the atmospheric density in the heterosphere has been provided by satellite drag data analysis. The first results showed that the density decreases at a slower rate above 100 km altitude than in the homosphere. Such a decrease of the density gradient results from an increase of the atmospheric scale height, i.e., a diminution of the mean molecular mass and an increase of the temperature with altitude. The temperature increase is necessarily related to an energy absorption by the atmospheric constituents. Moreover, the hydrodynamical regime of the atmosphere above 100 km is such that conduction provides a very effective way for the energy transport (Spitzer, 1949; Bates, 1951). The first analysis of the time evolution of the atmosphere subject to heat conduction was made by Lowan (1955). The effect of a heat flow on the temperature gradient was demonstrated by Nicolet (1961), and the static diffusion models used for the interpretation of the satellite drag data (Jacchia, 1971) are a direct application of Nicolet's analysis. The time dependent solution given by Harris and Priester (1962) requires a hypothetical second heat source which is of the same order of magnitude as the solar UV heating. The second heat source of Harris and Priester (1962) is introduced in order to reduce the amplitude of the diurnal temperature variation and to shift the temperature maximum from 17 hr LT to 14 hr LT. Whereas the satellite drag data usually lead to a maximum of the density around 14 hr LT, it is now well established that the temperature obtained from incoherent backscatter measurements peaks around 17 hr LT. By introducing perturbations of the density and of the temperature at the base of the thermosphere, Rishbeth (1969) and Chandra and Stubbe (1970) attempted to explain this phase anomaly. It seems, however, that such an explanation is not fully satisfactory (Cummack and Butler, 1972). With a two dimensional time-dependent model, Mayr and Volland (1972) showed that a diurnal wind circulation shifts the maximum of the atomic oxygen concentration 1 or 2 hr before the temperature maximum. This controversial example indicates that some of the mechanisms responsible for the thermospheric structure are not completely understood.

Even if the numerical techniques were sufficiently developed to obtain a three dimensional solution of the conservation equations (mass, momentum, and energy), it would still be necessary to know exactly the heat sources and the heat sinks which can influence the behavior of the upper atmosphere. Some of these parameters are known qualitatively but there are still large uncertainties with regard to quantitative evaluation. Up to now, only solar UV heating and IR loss by O have been considered in the theoretical models. But it appears that other mechanisms such as tidal dissipa-

B. M. McCormac (ed.), Physics and Chemistry of Upper Atmospheres, 54–63.

tion (Lindzen and Blake, 1970) and Joule heating (Cole, 1971) cannot be neglected *a priori.*

2. Absorption Cross Sections

In a sunlit upper atmosphere, solar UV radiation is without any doubt an important energy source (Bates, 1951; Johnson, 1956; Nicolet, 1961). It is however necessary to investigate which wavelengths can be absorbed by the thermospheric constituents, i.e. by O, O_2, N_2, He and H. An analysis of the absorption cross sections combined with the total contents of each constituent shows that, above 100 km altitude, it is necessary to consider only the wavelength region from 1750 Å down to approximatively 80 Å. Ozone and O_2 are the most important absorbers above 1000 Å. Since we are dealing only with altitudes higher than 100 km, O_3 absorption is negligible and the absorption cross sections for O_2 can be taken from the analysis by Ackerman (1971) in the Schumann-Runge continuum. The O_2 absorption cross section varies from 2×10^{-19} cm^2 at 1750 Å, with a peak of 1.5×10^{-17} cm^2 at (1425 ± 25) Å, to 3×10^{-19} cm^2 around 1220 Å. Since the molecular oxygen total content reaches a value of 7×10^{16} molecules cm^{-2} around 115 km, it is clear that the maximum absorption in the Schumann-Runge continuum will occur below 120 km. It is therefor necessary to include this wavelength region in theoretical models for which the lower boundary conditions are adopted below 120 km.

The intense solar Ly-α radiation at 1216 Å can be neglected in the thermospheric thermal structure, since it penetrates into the mesosphere practically without any appreciable absorption. The much less intense Ly-β line at 1027.8 Å can, however, ionize O_2 in the E region since the absorption and ionization cross sections are respectively 1.6×10^{-18} cm^2 and 9.6×10^{-19} cm^2. The carbon C III line at 977 Å is absorbed by O_2 with a cross section of 4×10^{-18} cm^2.

Below 1000 Å, most of the atmospheric constituents are ionized and the experimental and theoretical determinations of the relevant cross sections do not always have the required accuracy for an aeronomical application. The available data have recently been reviewed by Hudson (1971). The measurements related to a continuum can usually be applied to the atmosphere. When a band spectrum is involved, it should, however, be necessary to take into account the rotational structure, particularly in the thermosphere where temperatures higher than 1000 K occur. An example of such a situation is given by the N_2 spectrum between 910 Å and 796 Å. In this wavelength region a complex band structure appears and the absorption cross section varies approximatively between 10^{-19} cm^2 and 10^{-16} cm^2 (Huffman *et al.*, 1963; Cook and Metzger, 1964; Samson and Cairns, 1964; Carter, 1972). This kind of difficulty was already pointed out by Nicolet and Swider (1963) for ionospheric problems.

Table I gives the adopted absorption cross sections between 910 Å and 80 Å (Nicolet, 1969). The wavelength intervals correspond respectively to the first ionization potential of O (910 Å), to the first ionization potential of N_2 (796 Å), to the second (732 Å) and to the third (665 Å) ionization potential of O. The other limits

TABLE I

Absorption cross sections (cm^2)

Wavelength (Å)	O	O_2	N_2	He	H
910–796	4.0×10^{-18}	7.5×10^{-18}	see text	–	5.5×10^{-18}
796–732	4.0×10^{-18}	2.0×10^{-17}	2.0×10^{-17}	–	4.0×10^{-18}
732–665	7.5×10^{-18}	2.0×10^{-17}	2.3×10^{-17}	–	3.2×10^{-18}
665–375	1.1×10^{-17}	2.5×10^{-17}	2.3×10^{-17}	6.0×10^{-18}	1.5×10^{-18}
375–275	8.0×10^{-18}	1.7×10^{-17}	1.4×10^{-17}	3.0×10^{-18}	3.0×10^{-19}
275–150	3.8×10^{-18}	7.5×10^{-18}	5.0×10^{-18}	1.0×10^{-18}	1.0×10^{-19}
150–80	1.8×10^{-18}	3.5×10^{-18}	2.2×10^{-18}	3.0×10^{-19}	3.0×10^{-20}

have been chosen to allow an extrapolation from the X-ray region. In Table I, no value is given for N_2 between 910 Å and 796 Å since the absorption cross section changes at least by two orders of magnitude in this wavelength region. In order to estimate the amount of energy absorbed by N_2, the 910 to 796 Å interval is subdivided by assuming that 5% of the available solar energy is absorbed with a cross section $\sigma = 1 \times 10^{-19}$ cm^2, 5% with $\sigma = 2.5 \times 10^{-19}$ cm^2, 10% with $\sigma = 5 \times 10^{-19}$ cm^2, 20% with $\sigma = 1 \times 10^{-18}$ cm^2, 20% with $\sigma = 5 \times 10^{-18}$ cm^2, 20% with $\sigma = 1 \times 10^{-17}$ cm^2, and 20% with $\sigma = 2 \times 10^{-17}$ cm^2. Using the absorption cross sections of Table I, it is possible to compute the transmission of the different wavelength regions through the

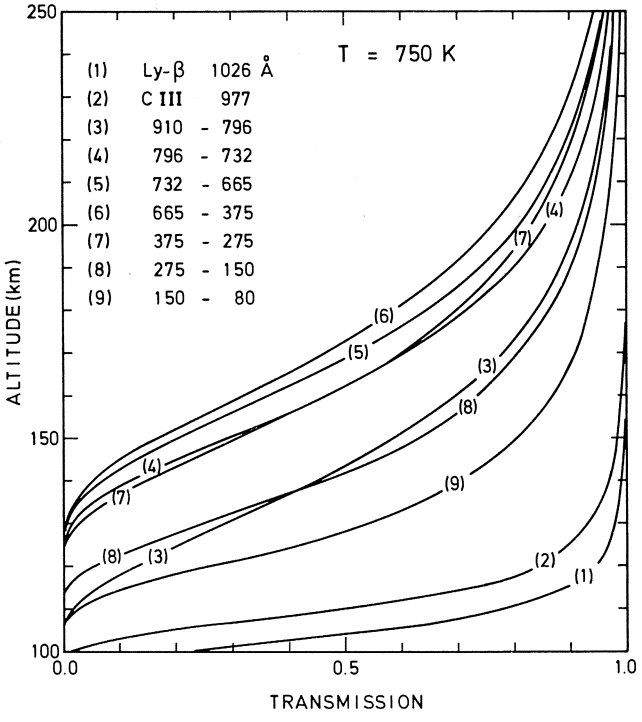

Fig. 1. Transmission of solar radiation for several wavelength bands in a 750 K atmospheric model. Overhead sun conditions.

upper atmosphere. Figure 1 gives an example of such a computation for an atmospheric model characterized by a 750 K thermopause temperature. It can be seen from Figure 1 that the amount of energy deposited by the Ly-β and the CIII lines is almost negligible above 120 km altitude. For the other wavelength intervals, unit optical depth (transmission = 0.369) is reached between 120 and 160 km. It is also clear that the absorption between 910 Å and 796 Å can play an important role. This is unfortunately the wavelength region where the N_2 absorption cross section has a very complex structure.

3. Solar Ultraviolet Flux

A quantitative evaluation of the heat production also requires accurate knowledge of the solar UV flux available at the top of the atmosphere. From the recent discussion of the solar UV flux by Ackerman (1971), it appears that the present available data in the Schumann-Runge continuum are not necessarely accurate enough for an unambiguous aeronomic application. It is, for instance, not well established whether or not a variation with solar activity occurs in the Schumann-Runge continuum. Below 1000 Å, there is an important variation with the solar cycle and the amplitude of this variation increases with decreasing wavelength. However, due to the presence of numerous chromospheric emission lines, it is difficult to establish a general correlation with the radio electric fluxes which do not necessarely come from the same solar regions (Hall and Hinteregger, 1970). Moreover, the absolute calibration of the measured UV fluxes is so difficult that it is not always easy to distinguish between real variation and instrumental effects.

In the Schumann-Runge continuum, the available energy flux is of the order of 15 erg cm^{-2} s^{-1}, whereas between 910 and 80 Å the total UV flux ranges from 1.7 to 4.5 erg cm^{-2} s^{-1} depending on the solar activity. Table II gives the UV fluxes for the same intervals as in Table I. The quoted variations are intended to represent real variations as well as experimental uncertainties. It should be noted that the experimental values recommended by Hinteregger (1970) for medium solar activity fall approximately in the middle of the range given in Table II.

4. Heat Sources

The heat production $P(\lambda, z)$ resulting from the absorption of a solar radiation of wavelength λ at an altitude z can be written

$$P(\lambda, z) = \sum_i \varepsilon_i(\lambda, z)\, \sigma_i(\lambda)\, n_i(z)\, E_{UV}(\lambda)\, e^{-\tau(\lambda, z)}, \tag{1}$$

where $\sigma_i(\lambda)$ is the absorption cross section of the constituent with concentration n_i. The summation is taken over all the components which can absorb the energy flux $E_{UV}(\lambda)$ available at the top of the atmosphere. The heating efficiency $\varepsilon_i(\lambda)$ represents the fraction of the UV energy which is transformed into heat. The optical

TABLE II

Possible solar UV fluxes (erg cm^{-2} s^{-1})

λ (Å)	E_{UV} (erg cm^{-2} s^{-1})	λ (Å)	E_{UV} (erg cm^{-2} s^{-1})
910–796	$(2.6 \pm 0.9) \times 10^{-1}$	375–275	$(8.4 \pm 3.7) \times 10^{-1}$
796–732	$(3.9 \pm 1.3) \times 10^{-2}$	275–150	$(1.4 \pm 0.6) \times 10^{0}$
732–665	$(2.1 \pm 0.7) \times 10^{-2}$	150–80	$(2.4 \pm 1.4) \times 10^{-1}$
665–375	$(3.4 \pm 1.6) \times 10^{-1}$		

depth $\tau(\lambda, z)$ is defined by

$$\tau(\lambda, z) = \sum_i \int_z^\infty n_i(z)\, \sigma_i(\lambda)\, F\, dz, \tag{2}$$

where the optical depth factor F is simply $\sec\chi$, when the solar zenith distance χ is less than 75°. For greater solar zenith distances F is given by the so-called Chapman function which takes the earth's curvature into account. Several practical approximations of F are available in the literature (Fitzmaurice, 1964; Swider, 1964). The total heating production over a certain wavelength interval is obtained by integration of Equation (1) over λ.

When the heating efficiencies ε_i are unity, Equation (1) gives the amount of energy absorbed by the atmosphere. Figure 2 shows the results for overhead sun ($F = \sec\chi = 1$) in two atmospheric models characterized by thermopause temperatures of 750 and 2000 K, respectively. The solar UV flux is identical in the Schumann-Runge conti-

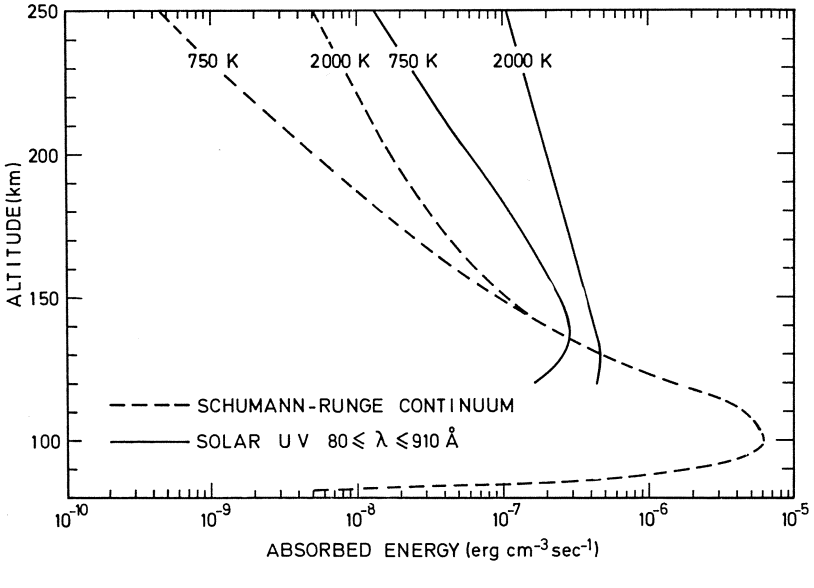

Fig. 2. Absorbed energy for overhead sun conditions in two atmospheric models with thermopause temperatures of 750 and 2000 K.

nuum for the two models. Between 80 and 910 Å, the minimum values of Table II are used for the 750 K model whereas the maximum values are adopted for the 2000 K model. Below 130 km altitude, the heating in the Schumann-Runge continuum is predominant. The heating efficiency, however, is less than one, since part of the available energy in the Schumann-Runge continuum is used for the photodissociation of molecular oxygen according to the process

$$O_2 + h\nu\,(\lambda < 1750\ \text{Å}) \rightarrow O\,(^3P) + O\,(^1D). \tag{3}$$

Any amount of energy above the dissociation threshold of 7.047 eV ($\lambda = 1750$ Å) should appear on the dissociation products. Furthermore, the metastable atom $O(^1D)$ can be deactivated to its ground state $O(^3P)$ by releasing an energy of 1.967 eV. Johnson and Gottlieb (1970) assume that any photon energy greater than 5.08 eV = 7.047–1.967 eV is transformed into heat. The heating efficiency in the Schumann-Runge continuum is then simply

$$\varepsilon_{S-R} = 1 - 4.1 \times 10^{-4}\,\lambda, \tag{4}$$

where λ is the incident photon wavelength in Å. The efficiency increases linearly with decreasing wavelength from 0.28 at 1750 Å to 0.59 at 1026 Å. In a more detailed analysis (Izakov, 1970; Izakov and Morozov, 1970), collisional deactivation of $O(^1D)$ and of $O_2(b^1\Sigma_g^+)$ as well as radiative emissions from excited states are taken into account. Izakov and Morozov (1970) suggest an average efficiency of 0.3 between 1750 Å and 1350 Å. With this value, Figure 2 shows that a maximum heat production of 1.8×10^{-6} erg cm^{-3} s^{-1} occurs around 100 km due to the absorption in the Schumann-Runge continuum.

Below the first ionization potential of O_2 at 1026 Å, it is very difficult to estimate the efficiency since the UV radiation is simultaneously absorbed by O, O_2, and N_2. Photoelectrons can also produce secondary ionizations and excitations. Chemical reactions between ionized species and neutral particles lead to a very complex procedure for the energy transfer. Furthermore, thermal energy is not necessarily released at the height where absorption of the solar radiation occurs, since particle transport phenomena can be involved in an appreciable way. The heating efficiency could also depend on solar activity since the relative abundance of the atmospheric constituents is variable during a solar cycle. An order of magnitude of the amount of heat produced below 1000 Å can be obtained by multiplying the absorbed energies of Figure 2 by 0.3. It should also be realized that the daily solar UV heat production depends strongly on the geographic latitude and on the season. These factors are involved in Equation (2) through the optical depth factor F which changes as a function of latitude, solar declination, and local time.

Among the other heat sources which could play a role in the heterosphere, one should consider Joule heating (Cole, 1971) which is accompanied by viscous heat dissipation. Tidal dissipation from below has also been suggested as a non negligible heat source (Lindzen and Blake, 1970), but the excitation mechanism has not yet been fully explored (Kato, 1971).

Joule heating results from electric currents in the ionosphere. Convection E fields

originate in the magnetosphere and lead then to complex movements of the ionospheric plasma in the earth's magnetic field. Fedder and Banks (1972) have shown that energies of the order of 10^{-6} erg cm^{-3} s^{-1} can be deposited over the polar cap in the E region. Such values are higher than the absorbed energy for $\lambda<910$ Å given on Figure 2 and they are comparable to the energy absorbed in the Schumann-Runge continuum. It is still necessary, however, to determine which fraction of this energy can be converted into heat. Up to now Joule heating has not been introduced in theoretical models. It appears however that such a high latitude energy source could influence the global thermospheric structure through imporant horizontal movements.

5. Heat Sinks

Among the various atmospheric components which can play a role in the thermal structure of the heterosphere, only O has a permanent magnetic dipole moment. Therefore, IR emission of O can lead to an energy loss process in the heat balance. The excitation potentials of the two upper levels of the ground state O(^{3}P) are of the same order of magnitude as the thermal energy of the atmospheric constituents. Infrared emissions are possible at 63 and at 147 μm (Bates, 1951). The intensity of the 147 μm emission is, however, negligible. For temperatures between 300 and 2000 K the IR flux at 63 μm is given approximately (Kockarts, 1971) for an optically thin atmosphere, by

$$L_{63\,\mu}(z) \simeq 7 \times 10^{-19} \int_z^\infty n(\mathrm{O})\,\mathrm{d}z \quad (\mathrm{erg\ cm^{-2}\ s^{-1}}) \tag{5}$$

which leads to a cooling flux of 1.3 erg cm^{-2} s^{-1} at 120 km. Equation (5) however overestimates the IR loss by several orders of magnitude at 100 km and by 10 to 20% at 150 km. Accurate results require the solution of a radiative transfer equation since O is not optically thin at 63 μm below 150 km. In this case the cooling flux ranges between 0.1 and 0.2 erg cm^{-2} s^{-1} for thermopause temperatures of 750 and 2000 K. A detailed discussion of the radiative transfer solution is given by Kockarts and Peetermans (1970). In any case, it appears that the IR loss is not sufficient to avoid the buildup of very large temperature gradients around 120 km.

6. Energy Balance

Swartz *et al.* (1971) studied the equatorial energy balance for an empirical model based on incoherent scatter temperature measurements and satellite drag density determinations. With a heating efficiency of the order of 0.4, Hinteregger's (1970) UV input fluxes were about 10% less than the total losses including the horizontal transport effects.

The most simple one-dimensional heat conduction equation is

$$\varrho c_v \frac{\partial T}{\partial t} + \frac{\partial E}{\partial z} = P - L \tag{6}$$

where the heat conduction flux E is given by

$$E = -\varkappa \frac{\partial T}{\partial z}. \tag{7}$$

In these equations ϱ is the total density, c_v the specific heat at constant volume, and $\varkappa$ is the heat conductivity. With the UV flux of Table II and the IR loss, Equation (6) leads to a diurnal amplitude of the temperature greater than a factor of 2, as shown by the dashed curve on Figure 3. It is possible, however, to *simulate* the effect of lateral compressional heating at night and of expansive cooling during the day. This can be done by introducing into the second member of Equation (6) an arbitrary production or loss

$$P_c = A \exp\left[-\frac{1}{2}\left(\frac{z - z_0}{s}\right)^2\right], \tag{8}$$

where z_0 is the altitude of the maximum value for P_c. With $s = 50$ km and $A = 8 \times 10^{-10}$ erg cm^{-3} s^{-1}, the integrated flux obtained from Equation (8) is only 0.1 erg cm^{-2} s^{-1}. Using the time dependent distribution shown on Figure 3 for the integrated flux, the solution of Equation (6) leads to the diurnal thermopause temper-

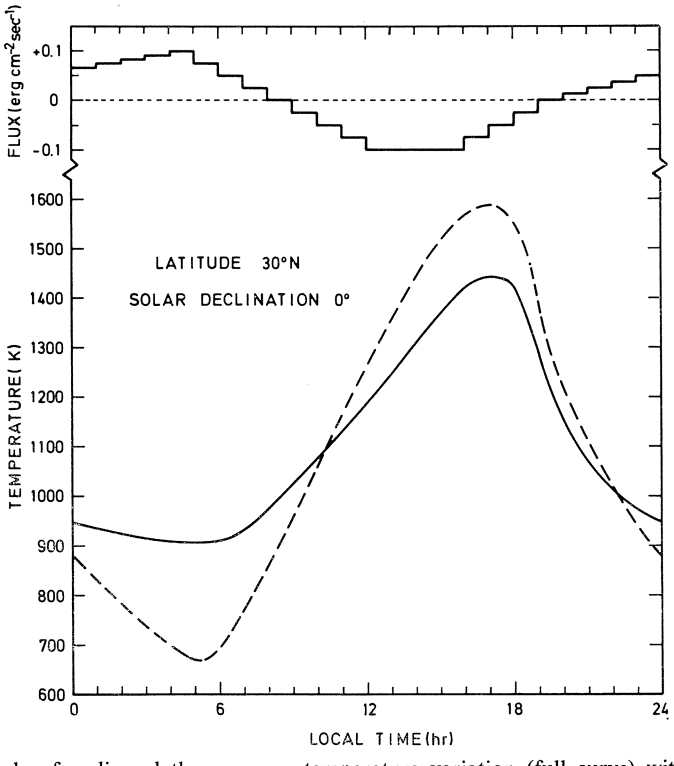

Fig. 3. Example of a diurnal thermopause temperature variation (full curve) with a small heat source or loss shown in the upper part of the figure (see Equation (8)). The dashed line corresponds to the case when only UV heating and IR loss are involved.

ature variation given by the full curve, when $z_0 = 350$ km in Equation (8). It is clear that the diurnal amplitude is strongly reduced. The total loss introduced through P_c during the day is approximatively equal to the total heat production during the night. The more or less arbitrary heat source (or loss) given on Figure 3 never exceeds 0.1 erg cm^{-2} s^{-1} whereas the maximum UV heating flux at 1200 LT is of the order of 2 erg cm^{-2} s^{-1} in this example. The additional source or loss introduced here is completely different in magnitude and in amplitude from the second heat source used by Harris and Priester (1962). It should be noted that even with P_c small compared to the UV heating below 910 Å, it is possible to build models in agreement with the incoherent scatter temperature measurements. The diurnal variation of P_c is a function of latitude and solar declination. No attempt has been made to fit any particular measurement and the Schumann-Runge continuum was not taken into account. When this wavelength region is included, turbulent downward heat transport must be included around 120 km to avoid too large temperature gradients below 150 km. This problem, however, is independent of the effect resulting from the term P_c.

At the present time, the general conservation equations have never been solved for a planetary upper atmosphere. It is almost impossible, therefore, to make a definite analysis of the heat balance. Furthermore, the heat sources and heat sinks are not known with enough accuracy. Continuous and accurate measurements of the solar UV spectrum are one of the major requirements for a good understanding of the mechanism responsible for the upper atmospheric thermal structure. The compressional heating at night and the expansive cooling during the day result from horizontal transports and it is difficult to make exact computations without solving the coupled three dimensional conservation equations. However, the use of a small nighttime production and daytime loss around 300 or 350 km can simulate horizontal energy transport.

References

Ackerman, M.: 1971, in G. Fiocco (ed.), *Mesospheric Models and Related Experiments*, D. Reidel Publishing Company, Dordrecht-Holland, p. 149.
Bates, D. R.: 1951, *Proc. Phys. Soc.* **64B**, 805.
Carter, V. L.: 1972, *J. Chem. Phys.* **56**, 4195.
Chandra, S. and Stubbe, P.: 1970, *Planetary Space Sci.* **18**, 1021.
Cole, K. D.: 1971, *Planetary Space Sci.* **19**, 59.
Cook, G. R. and Metzger, P. M.: 1964, *J. Chem. Phys.* **41**, 321.
Cummack, C. M. and Butler, P. M.: 1972, *Planetary Space Sci.* **20**, 289.
Fedder, J. A. and Banks, P. M.: 1972, *J. Geophys. Res.* **77**, 2328.
Fitzmaurice, J. A.: 1964, *Appl. Opt.* **3**, 640.
Hall, L. A. and Hinteregger, H. E.: 1970, *J. Geophys. Res.* **75**, 6959.
Harris, I. and Priester, W.: 1962, *J. Atmospheric Sci.* **19**, 286.
Hinteregger, H. E.: 1970, *Ann. Geophys.* **26**, 547.
Hudson, R. D.: 1971, *Rev. Geophys.* **9**, 305.
Huffman, R. E., Tanaka, Y., and Larrabee, J. C.: 1963, *J. Chem. Phys.* **39**, 910.
Izakov, M. N.: 1970, *Geomag. and Aeron.* **10**, 279.
Izakov, M. N. and Morozov, S. K.: 1970, *Geomag. Aeron.* **10**, 495.
Jacchia, L. G.: 1971, *Smithsonian Inst. Astrophys. Obs. Spec. Rep.* **332**.
Johnson F. S.: 1956, *J. Geophys. Res.* **61**, 71.
Johnson, F. S. and Gottlieb, B.: 1970, *Planetary Space Sci.* **18**, 1707.

Kato, S.: 1971, *Space Sci. Rev.* **12**, 421.
Kockarts, G.: 1971, in F. Verniani (ed.), *Physics of the Upper Atmosphere*, Editrice Compositori, Bologna, Italy, p. 389.
Kockarts, G. and Peetermans, W.: 1970, *Planetary Space Sci.* **18**, 271.
Lindzen, R. S. and Blake, D.: 1970, *J. Geophys. Res.* **75**, 6868.
Lowan, A. N.: 1955, *J. Geophys. Res.* **60**, 421.
Mayr, H. G. and Volland, H.: 1972, *J. Geophys. Res.* **77**, 2359.
Nicolet, M.: 1961, *Planetary Space Sci.* **5**, 1.
Nicolet, M.: 1969, private communication.
Nicolet, M. and Swider, W. Jr.: 1963, *Planetary Space Sci.* **11**, 1459.
Rishbeth, H.: 1969, *Ann. Geophys.* **25**, 495.
Samson, J. A. R. and Cairns, R. B.: 1964, *J. Geophys. Res.* **69**, 4583.
Spitzer, L., Jr.: 1949, in G. P. Kuiper (ed.), *The Atmospheres of the Earth and Planets*, The University of Chicago Press, Chicago, Illinois, p. 213.
Swartz, W. E., Rohrbaugh, J. L., and Nisbet, J. S.: 1971, *Ionospheric Research Sci. Rep. 383, Pennsylvania State University.*
Swider, W. Jr.: 1964, *Planetary Space Sci.* **12**, 761.